Zonal Momentum Budget of the Madden–Julian Oscillation: The Source and Strength of Equivalent Linear Damping

JIA-LIN LIN

NOAA–CIRES Climate Diagnostics Center, Boulder, Colorado

MINGHUA ZHANG

State University of New York at Stony Brook, Stony Brook, New York

BRIAN MAPES

NOAA–CIRES Climate Diagnostics Center, Boulder, Colorado

(Manuscript received 29 January 2004, in final form 21 October 2004)

ABSTRACT

Linear, dissipative models with resting base states are sometimes used in theoretical studies of the Madden–Julian oscillation (MJO). Linear mechanical damping in such models ranges from nonexistent to strong, since an observational basis for its source and strength has been lacking. This study examines the zonal momentum budget of a composite MJO over the equatorial western Pacific region, constructed using filtering and regression techniques from 15 yr (1979–93) of daily global reanalysis data. Two different reanalyses (NCEP–NCAR and ERA-15) give qualitatively similar results for all major terms, including the budget residual, whose structure is consistent with its interpretation as eddy momentum flux convergence (EMFC) in convection.

The results show that the MJO is a highly viscous oscillation, with a 3–5-day equivalent linear damping time scale, in the upper as well as lower troposphere. Upper-level damping is mainly in the form of large-scale advection terms, which are linear in MJO amplitude but involve horizontal and vertical background flow. Specifically, the leading terms are the advection of time-mean zonal shear by MJO vertical motion anomalies and advection of MJO wind anomalies by time-mean ascent. This upper-level damping in the western Pacific is mostly confined between 10°N and 10°S. In contrast, zonal wind damping in the lower troposphere involves EMFC (budget residual) and zonal mean linear meridional advection.

Stated another way, the strong upper-level damping necessitates upper-level geopotential height gradients to maintain the observed zonal wind anomalies over the time scales implied by the MJO's low frequency. The existence of the background flow thus tends to shift MJO temperature perturbations westward so that the warm anomaly ahead (east) of the convective center is shifted back into the convection. This shifting effect is fully realized only for anomalies with a period much longer than the 3–5-day damping time.

1. Introduction

Discovered by Madden and Julian (1971, 1972), the Madden–Julian oscillation (MJO) is the dominant intraseasonal mode of variability in tropical convection and circulation (e.g., Weickmann et al. 1985; Lau and Chan 1985; Salby and Hendon 1994; Wheeler and Kiladis 1999). It affects a wide range of tropical weather such as the onset and breaks of the Indian and Australian summer monsoons (e.g., Yasunari 1979; Hendon and Liebmann 1990) and the formation of tropical cyclones (e.g., Nakazawa 1986; Liebmann et al. 1994). It also drives teleconnections to the extratropics (e.g., Lau and Phillips 1986) and impacts some important extratropical weather (e.g., Higgins and Mo 1997; Higgins et al. 2000). On a longer time scale, the MJO is observed to trigger or terminate some El Niño events (e.g., Kessler et al. 1995; Takayabu et al. 1999; Bergman et al. 2001; Roundy and Kiladis 2005, manuscript submitted to *J. Climate*). Therefore, the MJO is important for both extended-range weather prediction and long-term climate prediction.

Tropical intraseasonal variability is poorly simulated

Corresponding author address: Dr. Jia-Lin Lin, NOAA–CIRES Climate Diagnostics Center, 325 Broadway, R/CDC1, Boulder, CO 80305.
E-mail: jialin.lin@noaa.gov

in general circulation models (GCMs). Typically, simulated phenomena are too weak and propagate too fast (e.g., Hayashi and Sumi 1986; Hayashi and Golder 1986, 1988, 1993; Lau et al. 1988; Slingo et al. 1996). To solve this problem, many theoretical studies have examined the feedback mechanisms that may affect the MJO's amplitude and phase speed, especially the wave–heating feedback mechanisms. Different types of heating parameterizations have been studied, such as wave–CISK (convective instability of the second kind: e.g., Lau and Peng 1987; Chang and Lim 1988), frictional wave–CISK (e.g., Wang 1988; Salby et al. 1994), WISHE (wave induced surface heat exchange; e.g., Emanuel 1987; Neelin et al. 1987), charge–discharge (e.g., Blade and Hartmann 1993; Hayashi and Golder 1997), and cloud–radiation interaction (Raymond 2001).

In these theoretical studies, linear, dissipative models were often used with the momentum equation linearized about a state at rest:

$$\frac{\partial u'}{\partial t} = -\frac{\partial \phi'}{\partial x} + fv' - \epsilon u' \tag{1}$$

$$\frac{\partial v'}{\partial t} = -\frac{\partial \phi'}{\partial y} - fu' - \epsilon v', \tag{2}$$

where u is the zonal wind, v is the meridional wind, ϕ the geopotential height, and f the Coriolis parameter. The mechanical damping is usually represented as a Rayleigh friction with a time scale of ϵ^{-1}. Such mechanical damping has been shown to affect the growth rate and phase speed of simulated intraseasonal oscillations. For example, in the case of a free Kelvin wave, Chang (1977) found that damping can significantly increase the intrinsic vertical wavelength and decrease the intrinsic phase speed. In a wave–CISK type model, Chao (1987) found that the phase speed of an intraseasonal oscillation decreases with increasing damping. In a WISHE model of the MJO, Neelin et al. (1987) found that the growth rate of the unstable Kelvin modes significantly decreases with increasing mechanical damping, and this was later confirmed by Neelin and Yu (1994) and Goswami and Rao (1994). However, the choices of damping magnitude in these and other theoretical models vary over a wide range, from highly viscous (e.g., 1 day in Chao 1987), to weakly viscid (e.g., 25 days in Salby et al. 1994), to totally inviscid (e.g., Xie 1994).

The choice of linear damping magnitude in the frictional boundary layer is also important for the frictional Wave–CISK theory of the MJO (e.g., Wang and Rui 1990a; Wang and Li 1994; Moskowitz and Bretherton 2000). Wang and Li (1994) and Moskowitz and Bretherton (2000) both show that the instability of the simulated MJO-like mode is very sensitive to the value of linear damping, and to the thickness of the frictional layer. Using a 0.3-day damping rate and a 100-mb-thick frictional layer, Wang and Rui (1990a) got a highly unstable MJO-like mode. On the other hand, using a 1.3-day damping rate and a 50-mb-thick frictional layer, Moskowitz and Bretherton (2000) got a growth rate that is only tenth of that in Wang and Rui (1990a). Therefore how large the equivalent linear damping is in the atmospheric boundary layer determines whether frictional Wave–CISK is important for the amplification of the MJO.

The budget terms, which are not explicitly expressed in the linearized Eqs. (1) and (2), include the advective tendency and the effect of convective eddy momentum transport (CMT, also called "cumulus friction" in some previous studies), and therefore they are the possible sources of equivalent linear mechanical damping from the viewpoint of the linear, dissipative models that were often used in developing the MJO theories.[1]

In MJO models that did use a strong damping, the source of the damping was usually assumed to be the CMT. The importance of CMT for synoptic-scale waves has been shown in both the momentum budget (Stevens 1979) and the vorticity budget (e.g., Reed and Johnson 1974; Shapiro 1978; Stevens 1979; Esbensen et al. 1982; see review by Sui and Yanai 1986). For the MJO, the importance of CMT was also shown by two recent observational studies (Houze et al. 2000; Tung and Yanai 2002a, b). Using Doppler radar data collected by aircraft and ship radars during the Tropical Ocean Global Atmosphere Coupled Ocean–Atmosphere Response Experiment (TOGA COARE) field program, Houze et al. (2000) inferred the sense of mesoscale momentum transport in the "superconvective systems" in different phases of the MJO event. They found that this mesoscale momentum transport provides damping to the low-level zonal wind in the westerly onset phase, but acceleration during the mature westerly wind burst phase. Using TOGA COARE sounding array momentum budgets, Tung and Yanai (2002a,b) studied the area-averaged CMT, which includes both the convective-scale momentum transport and the mesoscale momentum transport. They found that the area-averaged CMT is strongly modulated by the MJO event and provides acceleration in the westerly onset phase, but damping in the westerly wind burst phase: opposite in sign to the effect of mesoscale momentum transport. In these two studies, the magnitude of CMT effect was not compared with those of the other momentum budget terms at the MJO time scale, and the equivalent damping strength was not estimated. Weickmann et al. (1997) calculated the vertically integrated angular momentum budget for the MJO and found that the advective tendency is a dominant budget

[1] In the case of nonlinear models, on the other hand, the advective tendency is explicitly included in the momentum equation, and thus is not represented by the linear damping.

term. This suggests that the advective tendency may be another important source of mechanical damping.

The purpose of this study is to evaluate the sources and strength of equivalent linear mechanical damping in the observed MJO. To do this, we calculate the MJO momentum budget using 15 years of daily reanalysis data and then identify the damping term in (1) with the terms proportional to u' in the full zonal momentum equation. Because the MJO circulation near the equator is dominated by the zonal wind, we focus on the zonal momentum budget. The main budget uncertainties associated with pressure gradient forces and advection terms are examined by 1) comparing between National Centers for Environmental Prediction (NCEP) and European Centre for Medium-Range Weather Forecasts (ECMWF) reanalyses, whose consistencies gave us more confidence and 2) constructing long-term (15 yr) MJO composite and considering only the statistically significant signals, which are likely real signals unless the reanalyses have errors coherent with the MJO.

The datasets used in this study are described in section 2. The time filtering and intraseasonal composite (regression) methods are described in section 3. The zonal momentum budget results are reported in section 4. Summary and discussions are given in section 5.

2. Data

The datasets used include 15 years (1979–93) of daily reanalyses data from two different centers: NCEP (Kalnay et al. 1996) and ECMWF [the 15-yr ECMWF Re-Analysis (ERA-15); Gibson et al. 1997]. The variables used include upper-air wind, geopotential height, and vertical pressure velocity on pressure surfaces. The horizontal resolution is 2.5° latitude × 2.5° longitude. The zonal momentum budget is calculated for both reanalyses, following Carr and Bretherton (2001), based on the zonal momentum equation:

$$\frac{\partial u}{\partial t} = -u\frac{\partial u}{\partial x} - v\frac{\partial u}{\partial y} - \omega\frac{\partial u}{\partial p} + f(y)v - \frac{\partial \phi}{\partial x} + X, \quad (3)$$

where u is the grid-resolved zonal wind, v the meridional wind, ω the vertical pressure velocity; x and y are east–west and north–south distance, f the Coriolis parameter, and ϕ the geopotential. Here X represents accelerations due to all subgrid-scale processes. Each budget term except X was calculated using daily average data at each 2.5° grid point; X is computed as the residual, meaning that all errors in the other terms are included in its observational estimate, requiring caution in interpretation. Derivatives were evaluated using three-point central differencing. The results were then averaged to pentad data along the equator (between 5°N and 5°S) with a zonal resolution of 10° longitude.

For constructing the MJO composite, we also used 15 years (1979–93) of pentad CMAP precipitation data (Xie and Arkin 1997) averaged along the equator (between 5°N and 5°S).

3. Method

The MJO is a broadband phenomenon, with an averaged period of 45 days but a fairly wide spread from 20 to 80 days (see review by Madden and Julian 1994). Its deep convection signal is dominated by wavenumber 1–6, while its circulation signal is dominated by wavenumber 1 (e.g., Salby and Hendon 1994; Wheeler and Kiladis 1999). The variance of its deep convection signal has two centers: western Pacific and eastern Indian Ocean. Over these two centers, the MJO propagates eastward with a slow phase speed of about 5 m s^{-1} (e.g., Wheeler and Kiladis 1999; Lin et al. 2004).

These characteristics were used to isolate the MJO signal. Lin et al. (2004) discussed the different methods used in previous observational and modeling studies. The different methods often give qualitatively similar results in terms of propagation characteristics and phase difference among different variables. This consistency is because intraseasonally filtered deep convection along the equator is dominated, both in number and strength, by coherent eastward propagating events (Wang and Rui 1990b). Linear composite methods used in most of the previous studies (e.g., phase sum, correlation, regression) are apparently dominated by these strong eastward propagating events. The method used in this study is similar to that used in Lin et al. (2004) and Lin and Mapes (2004). The procedure is as follows.

1) The zonal means were first removed from all datasets. The dynamical signal associated with the MJO heating has two distinct components: a "forced response" in the Eastern Hemisphere that moves eastward with the heating anomaly at a phase speed of about 5 m s^{-1}, and a "propagating response" in the Western Hemisphere that is excited in and radiated away from the heating anomaly at a phase speed of several tens of meters per second (e.g., Salby and Hendon 1994; Bantzer and Wallace 1996; Weickmann et al. 1997). It is primarily this propagating response that generates the zonal mean signals in MJO circulation anomalies. Because our focus is on wave–heating feedback, that is, the interaction between heating and the forced response, it is useful to remove the zonal mean signals caused by the propagating response. Nevertheless, we have repeated all our analysis to the data with zonal mean retained, and the basic features of zonal momentum budget are not changed.
2) The datasets were then filtered using a 30–70-day Murakami (1979) filter, whose response function was shown in Lin et al. (2004). The central frequency corresponds to a period of 45 days, with half

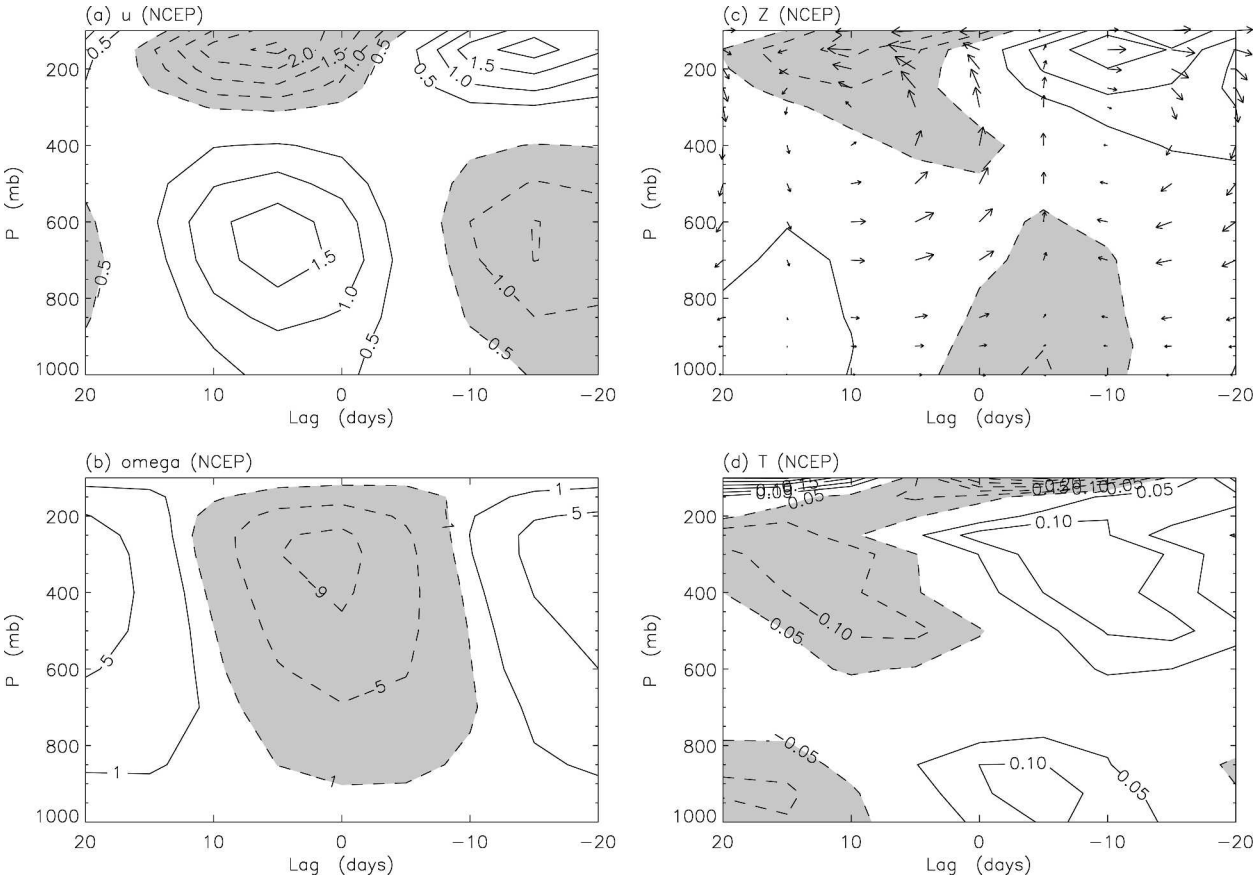

FIG. 1. The vertical structure of the MJO anomaly for (a) zonal wind (m s^{-1}), (b) vertical velocity (mb day^{-1}), (c) geopotential height (m), and (d) temperature (K) for the 15 years (1979–93) of NCEP reanalysis data averaged over 5°N–5°S, 150°–160°E. Negative values are shaded. The arrows in (c) are the wind vectors whose horizontal component is the zonal wind, and vertical component is the vertical velocity.

amplitude at periods of 30 and 70 days. We also tested the Lanczos filter (Duchan 1979), and the results were not sensitive.

3) For the master MJO index, we filtered the CMAP precipitation in time as above, and also in space, retaining wavenumbers 1–6.
4) To study the MJO phenomena in its two centers of variance, we averaged the datasets in two boxes: a western Pacific box between 5°N and 5°S, 150° and 160°E and an eastern Indian Ocean box between 5°N and 5°S, 80° and 90°E. For each box, and MJO composite was constructed using linear regression with respect to the filtered CMAP precipitation at the same box, and the regression coefficient was multiplied by one standard deviation of the filtered CMAP precipitation. The confidence level of linear correlation was estimated following Oort and Yienger (1996).
5) Regressions were done for all seasons of the year, as well as for individual seasons [December–February (DJF), March–May (MAM), June–August (JJA), and September–November (SON)].

4. Results

a. Vertical structure of the MJO at the equator

Before examining the MJO zonal momentum budget, we first look at the vertical structure of the MJO, which is important for understanding later the zonal momentum budget. The composite vertical structure of MJO in the western Pacific box is shown in Figs. 1 and 2. The time lag is with respect to the time of maximum precipitation. The time evolution is from the right to the left, showing the local evolution of measured variables as the eastward-moving MJO passes the measurement longitude. The zonal wind u (Fig. 1a) shows a simple two-layer structure with the upper layer out of phase with the lower layer. This two-layer structure is well known from many previous observations (e.g., Madden and Julian 1971, 1972; Weickmann et al. 1985; Knutson and Weickmann 1987).

One interesting subtlety is that the maxima of both the two layers are at higher altitudes than the 850-mb- and 200-mb levels used in many previous MJO studies. The maximum of the lower layer is around 600 mb (just

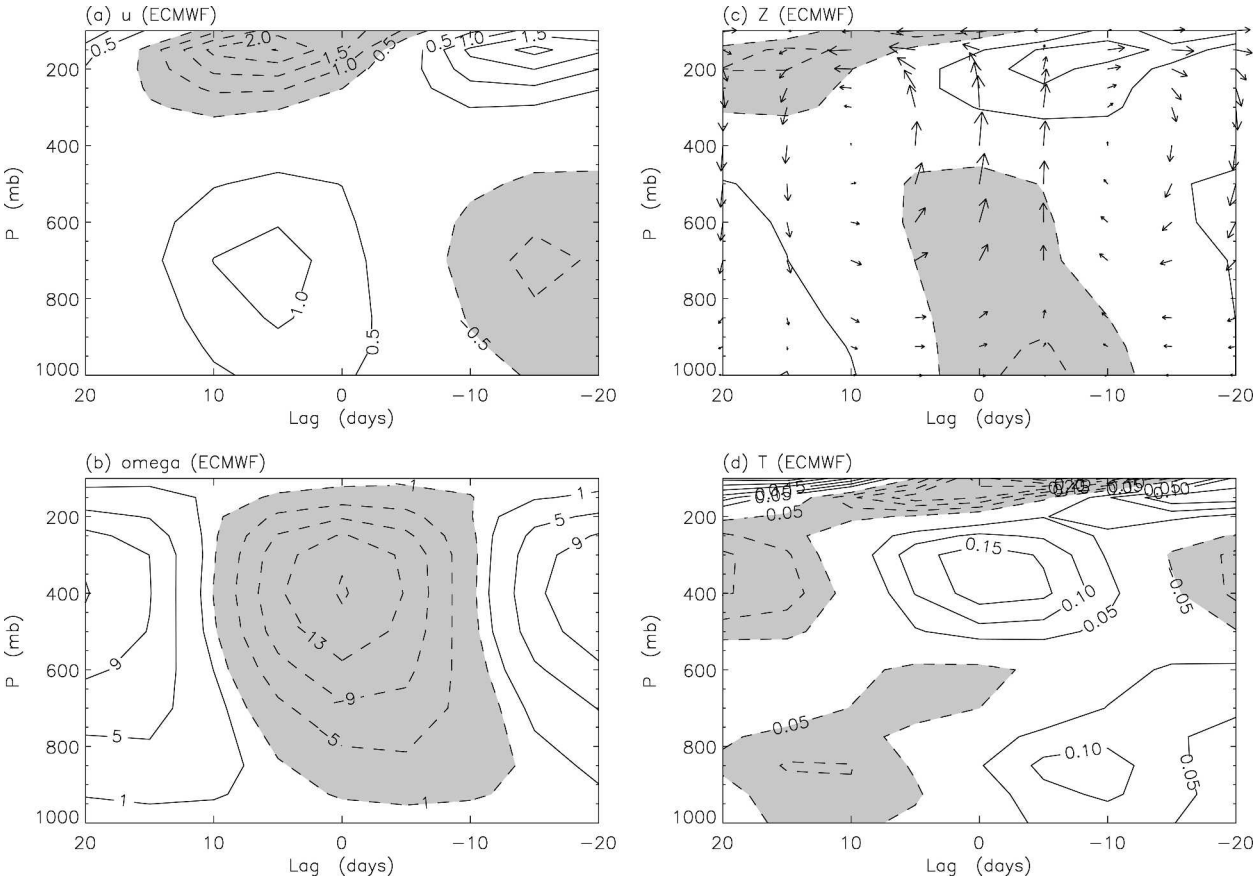

FIG. 2. As in Fig. 1 except for the ECMWF reanalysis data.

below the 0°C level), while that of the upper layer is around 150 mb (just below the tropopause). Similar results were obtained using GTS sounding data by Kiladis et al. (2005). Thus, at the time of maximum precipitation, the zonal convergence is just below the 0°C level and the zonal divergence is just below the tropopause. The zonal divergence pattern is shifted to the east relative to vertical motion and rainfall, indicative of the meridional component of divergence associated with the Rossby wave component of the flow. In the vertical, however, there is a consistency between the zonal divergence profile and the vertical motion (Fig. 1b), which concentrates high in the upper troposphere. This middle troposphere inflow and near-tropopause outflow structure are consistent with the top-heavy heating profile in the MJO shown in Lin et al. (2004).

The vertical motion shows a westward phase tilt with height. It develops first in the lower troposphere, which is consistent with boundary layer frictional convergence (not shown), and then shifts upward as it intensifies. This westward phase tilt of vertical motion is consistent with the westward phase tilt of the associated heating anomaly shown in Lin et al. (2004), which is caused by vertical phase tilts of convective heating in the earlier stages and stratiform heating in the later stages.

The geopotential height Z (contours in Fig. 1c) has a large amplitude in the near-tropopause outflow layer but a small amplitude in the middle-troposphere inflow layer. For clarity, the two-dimensional flow is also plotted using arrows in Fig. 1c; Z lags u at both the inflow and outflow layers, by about 5 days in the outflow layer and 10 days in the inflow layer. This phase shift is one of the features most different between the NCEP and ECMWF reanalyses (cf. Figs. 1c, 2c). The phase difference in the upper layer is smaller than those found by Kiladis and Weickmann (1992) and Hsu (1996). The reason is that we removed the zonal-mean component from all datasets while they did not, and our test using data retaining zonal mean showed that the zonal mean component in geopotential height increases the u and Z phase difference in the western Pacific (not shown).

Consistent with the geopotential height structure, the temperature (Fig. 1d) has its largest anomalies in three layers: the lower troposphere below 800 mb, the upper troposphere between 200 and 600 mb, and near the tropopause above 150 mb. The temperature anomaly in the upper troposphere is likely associated with the top-heavy heating profile shown in Lin et al. (2004), because modeling studies showed that the vertical structure of temperature perturbation follows that of heat-

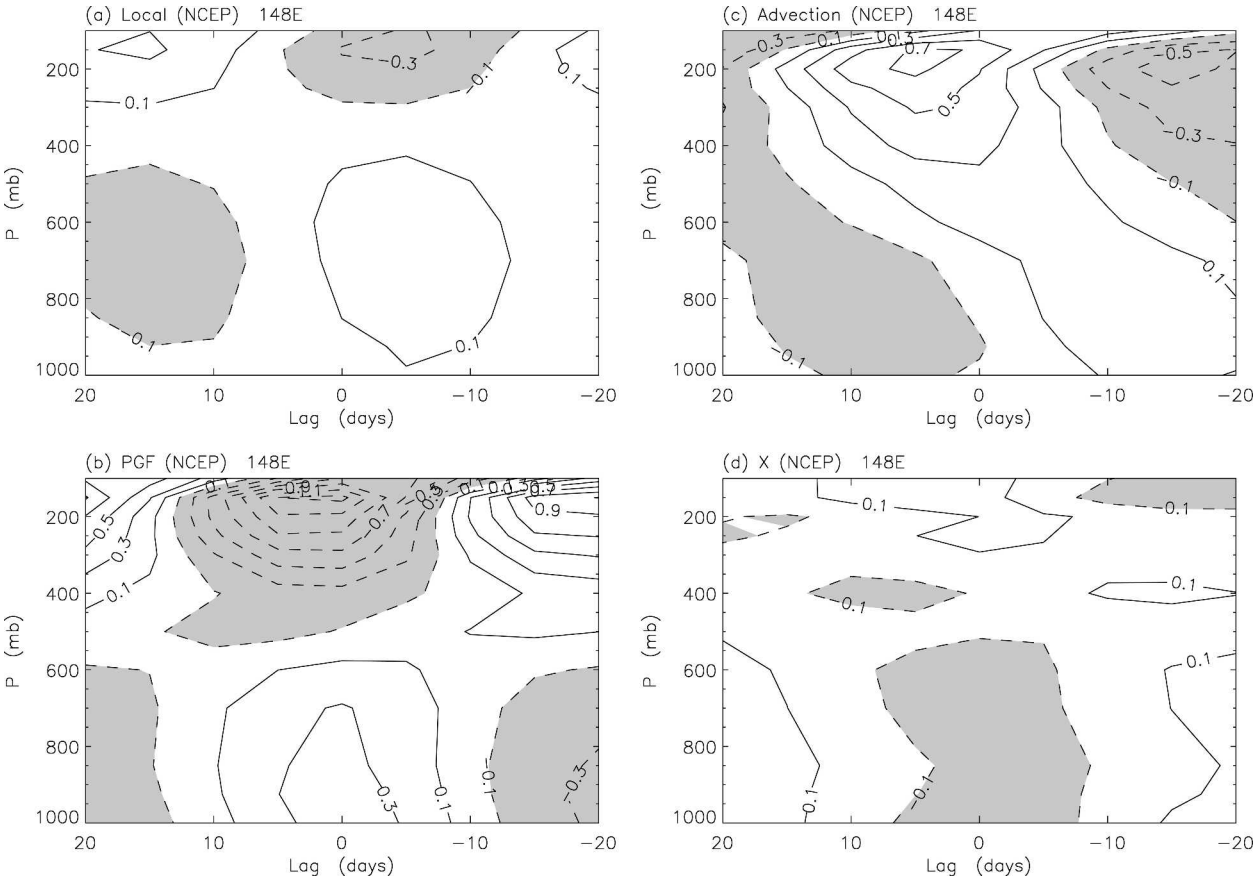

FIG. 3. Terms of the MJO zonal momentum budget: (a) local tendency ($\partial\tilde{u}'/\partial t$), (b) pressure gradient force $-(\partial\tilde{\phi}'/\partial x)$, (c) advection terms $[-u(\partial\tilde{u}'/\partial x) - v(\partial\tilde{u}'/\partial y) - \omega(\partial\tilde{u}'/\partial p)]$, and (d) the residual term $\widetilde{X}'$, for 15 yr (1979–93) of NCEP reanalysis data averaged over 5°N–5°S and 150°–160°E. Unit is m s^{-1} day^{-1}.

ing perturbation (e.g., Haertel and Kiladis 2004). The temperature anomaly near the tropopause is out of phase with that in the upper troposphere and has a larger amplitude than the later.

Composites constructed using 15 years (1979–93) of ECMWF reanalysis data show similar wave structure as the NCEP data (Fig. 2). We also checked the composites for each individual season (DJF, MAM, JJA, and SON). The wave structures are generally similar to the all-seasons composites.

In summary, the equatorial wave structure of the MJO has the following three characteristics:

1) it is associated with a vertical mode concentrated in the upper half of the troposphere, with middle-troposphere inflow and near-tropopause outflow at the time of maximum precipitation;
2) the vertical motion has a westward phase tilt with height; and
3) geopotential height lags zonal wind by about 5–10 days at both the inflow and outflow layers.

The phase difference between u and Z has implications for the zonal momentum budget. Equation (1) suggests that, when the damping is zero, the balance near the equator is simply between the local tendency and the pressure gradient force. In a neutral wave, this balance leads to an in-phase relationship between u and Z. Since zonal wind extrema in the MJO exist within pressure gradients, we can already anticipate that some other (damping) terms must contribute importantly to the zonal momentum budget.

b. Zonal momentum budget of the MJO

From Eq. (3) we can write the zonal momentum equation for intraseasonal anomalies of deviations from the zonal mean:

$$\frac{\partial\tilde{u}'}{\partial t} = -\frac{\partial\tilde{\phi}'}{\partial x} + f\tilde{v}' + \left(-u\frac{\tilde{\partial}u'}{\partial x} - v\frac{\tilde{\partial}u'}{\partial y} - \omega\frac{\tilde{\partial}u'}{\partial p}\right) + \widetilde{X}', \tag{4}$$

where the tilde denotes deviation from zonal mean, and primes denotes 30–70-day temporally filtered anomaly.

Major MJO zonal momentum budget terms at the equator (averaged between 5°N and 5°S, 150° and 160°E) are shown in Figs. 3 and 4 for NCEP and

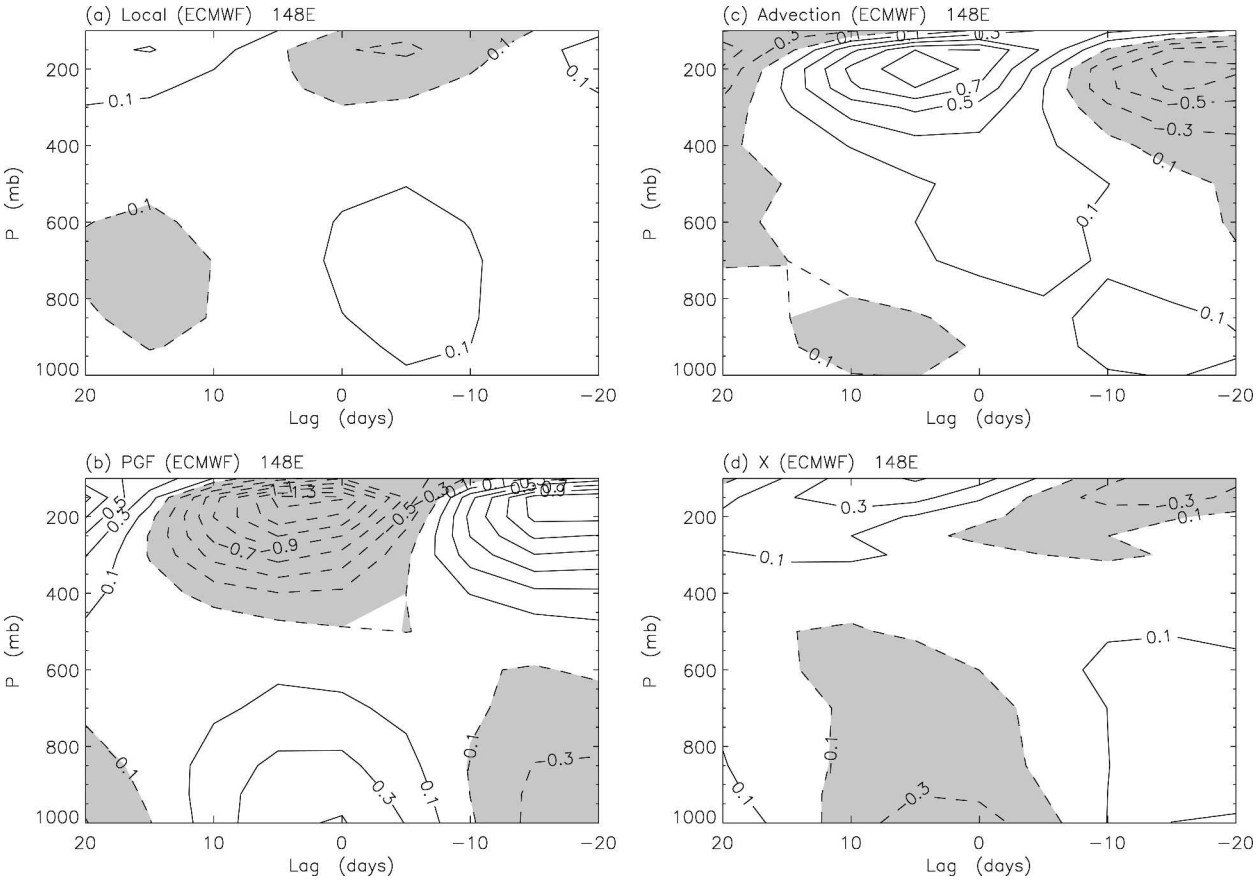

FIG. 4. As in Fig. 3 except for ECMWF reanalysis data.

ECMWF reanalyses, respectively. The Coriolis force is small near the equator and is not shown. The two different reanalyses show similar patterns for each of the three budget terms, giving us more confidence in the results. Moreover, only signals with correlation above the 95% confidence level are plotted in Figs. 3 and 4. These signals are likely real unless there are errors in the reanalyses that are systematically coherent with the MJO.

In the upper troposphere, the dominant balance is between the pressure gradient force and the advective tendency. The local tendency is much smaller, as is the budget residual. In the lower troposphere, the advective tendency and the budget residual are of similar amplitude as the local tendency and pressure gradient force. The MJO zonal momentum budgets for each individual season are similar to the all-seasons results (not shown).

The budget residual (Figs. 3d, 4d) shows a two-layer structure, with the residual near the tropopause out of phase with that in the lower troposphere. This is consistent with the vertical structure of budget residual in the TOGA COARE MJO events observed by Tung and Yanai (2002b, their Figs. 8b, 9b). During the westerly wind burst, the budget residual provides a damping to the zonal wind, which is also consistent with the TOGA COARE results. These results suggest that the budget residual from both reanalyses represent the effect of convective momentum transport (CMT). It is worth noting that the ERA-15 model had a parameterization of CMT, while the NCEP reanalysis model did not.

The large contribution of advective tendency to the MJO zonal momentum budget is subdivided into zonal, meridional, and vertical components in Fig. 5. In the upper troposphere, the advective tendency is mainly contributed by zonal (Fig. 5a) and vertical components (Fig. 5c), while that in the lower troposphere is mainly contributed by the meridional component (Fig. 5b). Each of these components contain both linear and nonlinear effects, which can be decomposed into (see the appendix)

$$-u\frac{\tilde{\partial}u'}{\partial x} = -[\tilde{u}]\frac{\partial \tilde{u}}{\partial x} - \tilde{u}'\frac{\partial[\tilde{u}]}{\partial x} + \text{other terms} \qquad (5)$$

$$-v\frac{\tilde{\partial}u'}{\partial y} = -[\tilde{v}]\frac{\partial \tilde{u}'}{\partial y} - \tilde{v}'\frac{\partial[\tilde{u}]}{\partial y} + \text{other terms} \qquad (6)$$

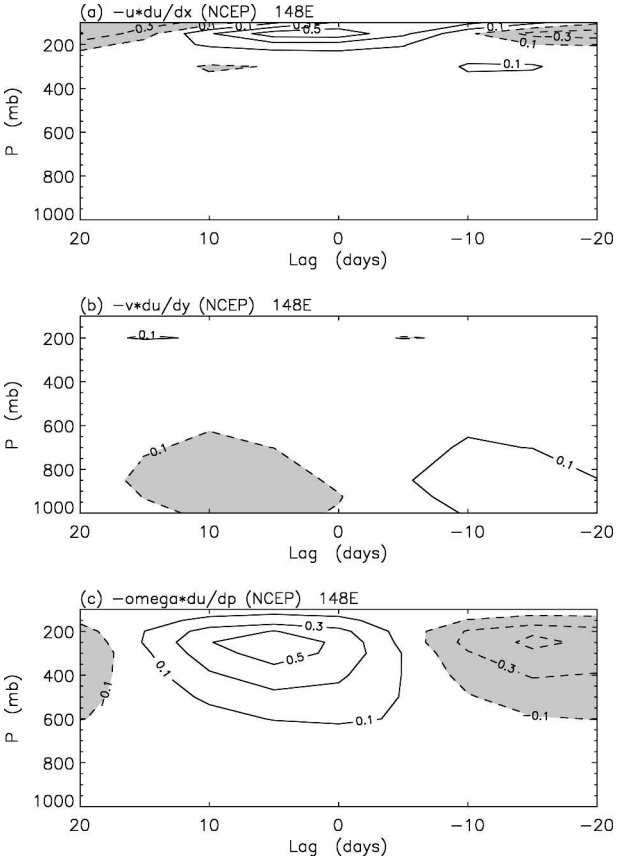

FIG. 5. As in Fig. 3 except for three advection terms for NCEP reanalysis data: (a) zonal advection $-u(\partial u'/\partial x)$, (b) meridional advection $-v(\partial u'/\partial y)$, and (c) vertical advection $-\omega(\partial u'/\partial p)$.

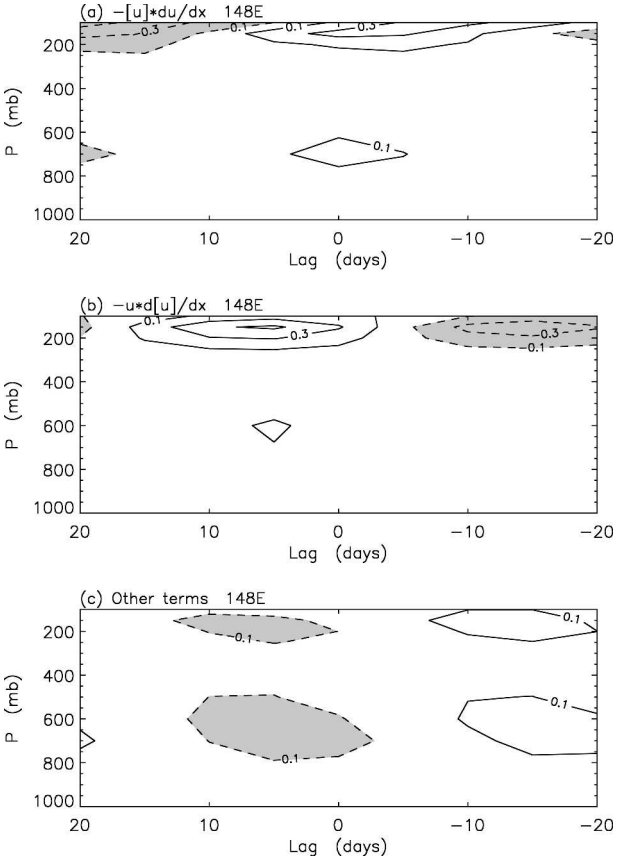

FIG. 6. As in Fig. 3 except for three components of the zonal advection term for NCEP reanalysis data: (a) $-[\tilde{u}](\partial u'/\partial x)$, (b) $-\tilde{u}'(\partial[\tilde{u}]/\partial x)$, and (c) other terms.

$$-\omega\frac{\partial\tilde{u}'}{\partial p} = -[\tilde{\omega}]\frac{\partial\tilde{u}'}{\partial p} - \tilde{\omega}'\frac{\partial[\tilde{u}]}{\partial p} + \text{other terms}, \quad (7)$$

where brackets denote time mean. On the right side of each equation, the first two terms are linear advection terms associated with time-mean zonal asymmetric flow, while the other terms include the linear terms associated with zonal-mean and the nonlinear terms (see the appendix). The first two linear terms were calculated from the corresponding time mean and the MJO anomalies, with the sum of all remaining terms left together as a (small) residual. For the zonal advection and the vertical advection, the time-mean was taken to be the 15-yr annual mean. For the meridional advection, because there is a strong seasonal variation in meridional wind, the time mean was taken to be 15-yr seasonal mean for one season, using DJF here as an example.

First we look at the decomposition of the zonal advection (Fig. 6) and the vertical advection (Fig. 7), which are important in the upper troposphere. The zonal advection (Fig. 6) is dominated by the first two linear terms, both of which contribute substantially to the budget. The vertical advection (Fig. 7) is also dominated by the first two linear terms, especially $-[\tilde{\omega}]\partial\tilde{u}'/\partial p$ (Fig. 7a). Therefore, the zonal momentum budget of the MJO is basically linear in the upper troposphere, but with an importantly nonresting basic state. This is consistent with the finding of Weickmann et al. (1997) that the vertically integrated MJO angular momentum budget is basically linear, since the vertically integrated momentum budget is mainly contributed by the upper troposphere.

The term $-[\tilde{u}]\partial\tilde{u}'/\partial x$, which describes the advection of the MJO anomaly by the time-mean zonal flow, cannot contribute to damping since it is in quadrature with $\tilde{u}'$. In contrast, $-[\tilde{u}]\partial\tilde{u}'/\partial x$, the advection of time-mean zonal flow by the MJO zonal wind anomaly, has an opposite phase with $\tilde{u}'$ in the upper troposphere, and therefore provides a damping. Meanwhile, $-[\tilde{\omega}]\partial\tilde{u}'/\partial p$, the advection of the MJO zonal wind anomaly by the time-mean vertical motion, tends to reduce the vertical windshear anomaly in the MJO, and therefore also provides a damping. The meridional advection (Fig. 8), which is important in the lower troposphere, is dominated by the terms other than the first two. Further

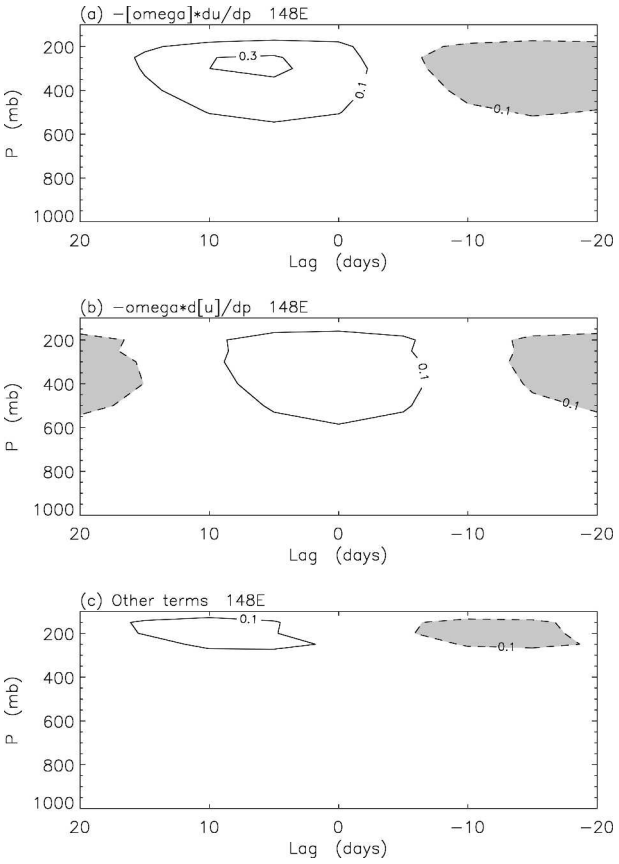

FIG. 7. As in Fig. 3 except for three components of the vertical advection term for NCEP reanalysis data: (a) $-[\tilde{\omega}](\partial\tilde{u}'/\partial p)$, (b) $-\tilde{\omega}'(\partial[\tilde{u}]/\partial p)$, and (c) other terms.

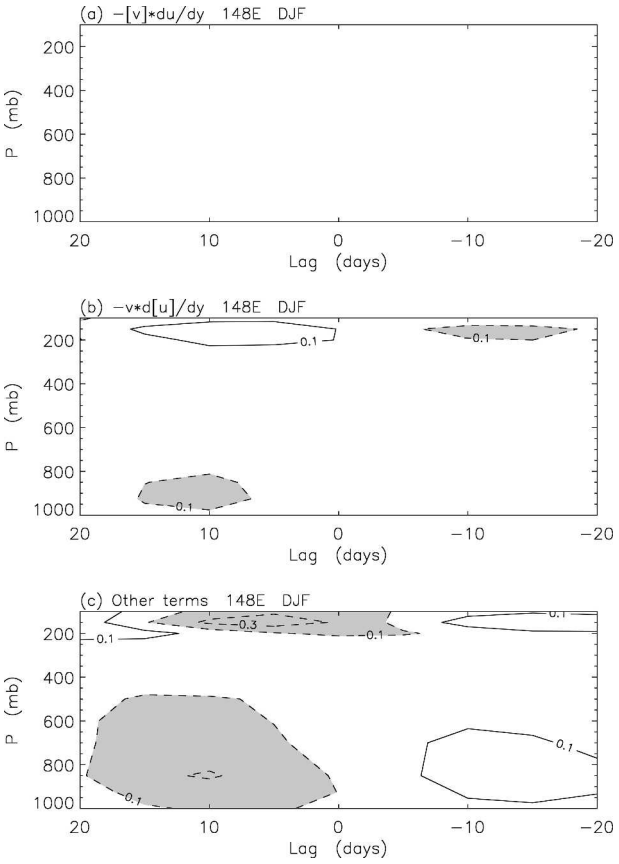

FIG. 8. As in Fig. 3 except for three components of the meridional advection term for NCEP reanalysis data for DJF season: (a) $-[\tilde{v}](\partial\tilde{u}'/\partial y)$, (b) $-\tilde{v}'(\partial[\tilde{u}]/\partial y)$, and (c) other terms.

analysis shows that it is actually dominated by the zonal mean linear term $-\tilde{v}'\partial[\overline{u}]/\partial y$ (not shown).

In summary, we find that the MJO zonal momentum budget near the equator can be simplified to

$$\frac{\partial\tilde{u}'}{\partial t} \approx -\frac{\partial\tilde{\phi}'}{\partial x} - [\tilde{u}]\frac{\partial\tilde{u}'}{\partial x} - \tilde{u}'\frac{\partial[\tilde{u}]}{\partial x} - [\tilde{\omega}]\frac{\partial\tilde{u}'}{\partial p} - \tilde{v}'\frac{\partial[\overline{u}]}{\partial y} + \widetilde{X}'. \quad (8)$$

c. *Understanding the linear advection terms in the upper troposphere*

The dominant linear advection terms in the upper troposphere owe their existence to the time-mean zonal wind $[\tilde{u}]$, zonal divergence $\partial[\tilde{u}]/\partial x$, and vertical velocity $[\tilde{\omega}]$. To help understand these terms, we plot their 15-yr (1979–93) climatological mean in Fig. 9. For consistency with the MJO anomaly, we plot here the zonal asymmetric components, but the zonal means are actually much smaller.

The warm pool region has abundant deep convection, associated with strong upward motion (Fig. 9a). The vertical velocity profile is very top-heavy and is, therefore, associated with strong upper-level zonal divergence concentrating in a thin layer near the tropopause (Fig. 9b). The upper-level zonal wind over the warm pool is easterly (Fig. 9c), consistent with the Gill (1980) pattern associated with a stationary heating source. The wind is strong within a thin layer near the tropopause because the zonal divergence is concentrated in this layer. Figure 9 only shows the annual mean, so the upper-level upward motion and zonal divergence are weaker over the eastern Indian Ocean. The long-term composite seasonal variation of upper-level vertical velocity, zonal divergence, and zonal wind (Fig. 10) shows that they are large over the eastern Indian Ocean during northern summer.

When the MJO travels in such a large-scale environment, three terms become important: 1) $-[\tilde{u}]\partial\tilde{u}'/\partial x$ (Fig. 6a) lags $\tilde{u}'$ (Fig. 1a) by a quarter cycle because the time-mean upper-level wind is easterly over the warm pool (Fig. 9c); 2) $-\tilde{u}'\partial[\tilde{u}]/\partial x$ (Fig. 6b) is out of phase with $\tilde{u}'$ because the time-mean upper level zonal wind gradient (zonal divergence) is positive over the warm pool (Fig. 9b), and is advected by the zonal wind anomaly in the MJO; 3) $-[\tilde{\omega}]\partial\tilde{u}'/\partial p$ (Fig. 7a) opposes

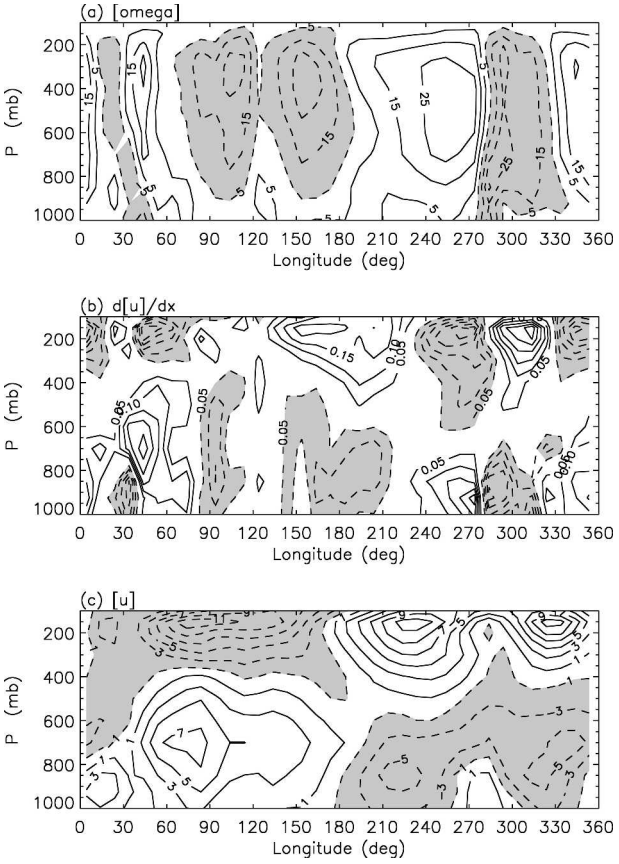

FIG. 9. Annual mean (a) $[\tilde{\omega}]$ (mb day^{-1}), (b) $(\partial[\tilde{u}]/\partial x)$ (day^{-1}), and (c) $[\tilde{u}]$ (m s^{-1}) for 15 years (1979–93) of NCEP reanalysis data along the equator (5°N–5°S).

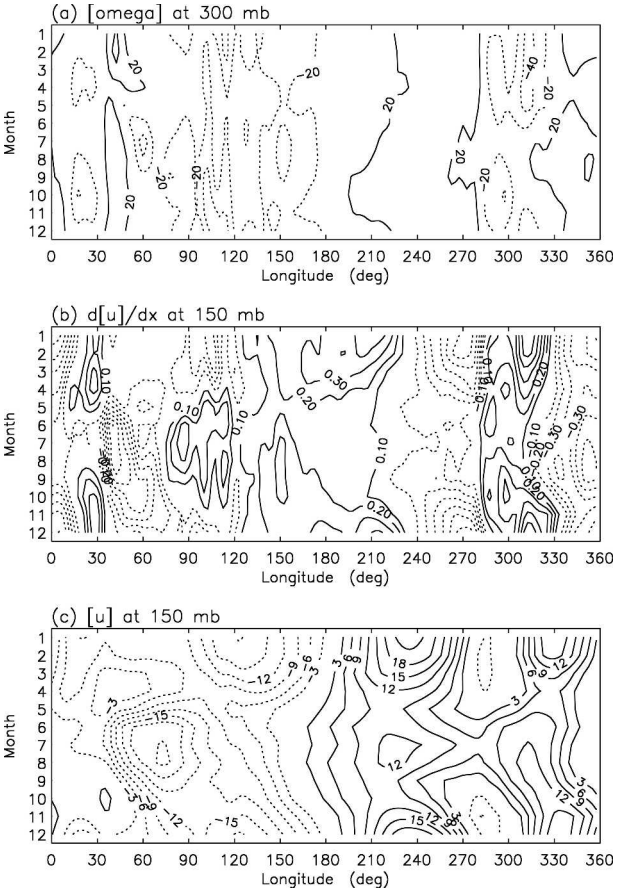

FIG. 10. Seasonal variation of (a) $[\tilde{\omega}]$ (mb day^{-1}) at 300 mb, (b) $(\partial[\tilde{u}]/\partial x)$ (day^{-1}) at 150 mb, and (c) $[\tilde{u}]$ (m s^{-1}) at 150 mb for NCEP reanalysis data along the equator (5°N–5°S).

the upper-level $\tilde{u}'$ (Fig. 1a) because zonal wind shear $\partial\tilde{u}'/\partial p$ is in phase with upper-level $\tilde{u}'$ and the time-mean vertical motion is upward (negative $[\tilde{\omega}]$, Fig. 9a).

A simple scale analysis clarifies the magnitudes of these terms and of local rate of change. The basic scales for the MJO and time-mean flow are

$T \approx 40$ days period
$L \approx 4 \times 10^7$ m zonal wavelength
$[\tilde{u}] \approx 10$ m s^{-1} time-mean upper-level zonal wind
$\partial[\tilde{u}]/\partial x \approx 0.2$ day^{-1} time-mean upper-level zonal divergence.

From these scales we can estimate the magnitude of the local tendency and the dominant linear zonal advection terms:

$$\frac{\partial\tilde{u}'}{\partial t} \approx 2\tilde{u}'/(0.5T) \approx \tilde{u}'/(10 \text{ days})$$

$$-[\tilde{u}]\frac{\partial\tilde{u}'}{\partial x} \approx [\tilde{u}] \times 2\tilde{u}'/(0.5L) \approx \tilde{u}'/(10 \text{ days})$$

$$-\tilde{u}'\frac{\partial[\tilde{u}]}{\partial x} \approx \tilde{u}'/(5 \text{ days}).$$

Therefore, the linear zonal advection term is larger than the local tendency. Because the vertical advection terms enhance the zonal advection terms, the total advective tendency (Fig. 3c), when scaled using $\tilde{u}'$ (Fig. 1a), is equivalent to a time scale of 2–3 days, which is much shorter than the 10-day time scale of local tendency. Therefore, the dominant balance between advective tendency and pressure gradient force in the upper troposphere is a physically sensible feature for the MJO.

d. Equivalent linear damping

To get quantitative estimates of the equivalent linear damping strength in the MJO, we regressed the MJO anomalies of the budget terms to the MJO zonal wind anomaly (Fig. 11). When a budget terms is in phase with (or in opposite phase to) the zonal wind, it provides a driving (or damping). The unit of the regression coefficient is day^{-1}—that is, the reciprocal of the coefficient gives the damping time scale in the unit of days. The corresponding correlation coefficient indicates

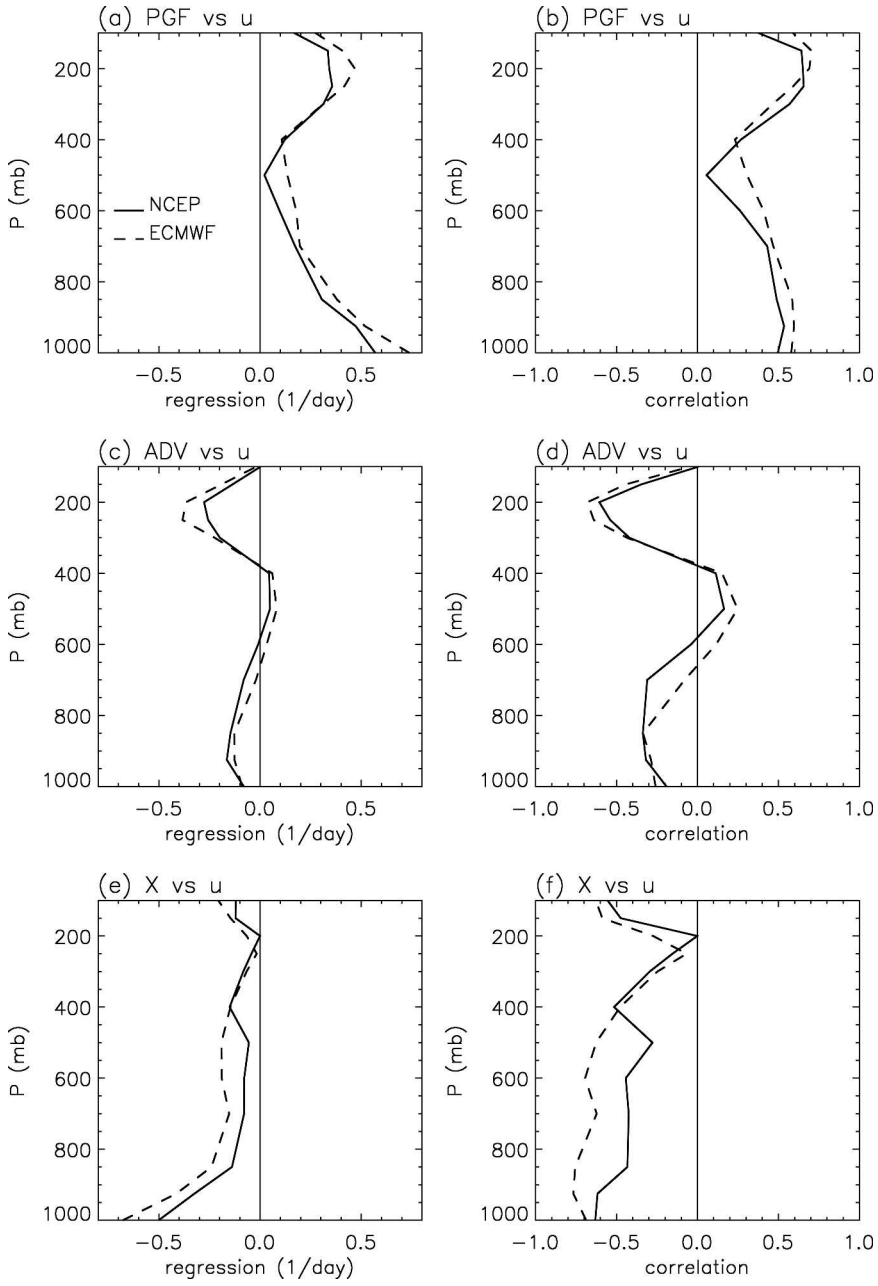

FIG. 11. Vertical profile of linear regression coefficient of the MJO (a) pressure gradient force anomaly, (c) advective tendency anomaly, and (e) budget residual anomaly, with respect to the zonal wind anomaly at the same level for 15 years (1979–93) of NCEP (solid line) and ECMWF (dashed line) reanalyses data averaged over 5°N–5°S, 150°–160°E. The corresponding correlation coefficients are shown in (b), (d), and (f), respectively.

how well the budget term is represented by a linear damping.

The pressure gradient force (Fig. 11a) provides a driving with a time scale of 2–3 days in the upper troposphere (150–300 mb), and 3–5 days in the lower troposphere (below 700 mb). This strong forcing cannot be balanced by the local tendency, which, as shown in section 4c, has a time scale of about 10 days. The Coriolis force is also small near the equator. Therefore, some strong dampings are needed to balance the pressure gradient force.

In the upper troposphere, the damping mainly comes from the advective tendency (Fig. 11c), which, as shown in section 4b, includes $-\tilde{u}'[\partial(\tilde{u})/\partial x]$ and $-[\tilde{\omega}](\partial\tilde{u}'/\partial p)$. The subgrid term X (Fig. 11e) also contributes slightly near the tropopause. In the lower troposphere, the

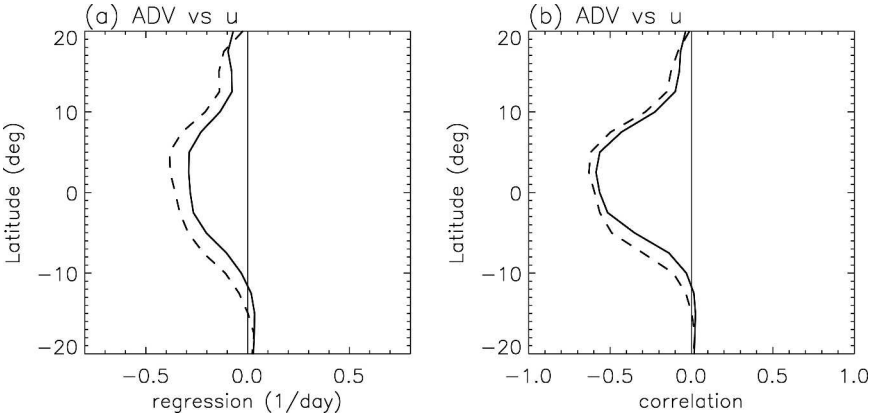

FIG. 12. Meridional profile of (a) linear regression coefficient and (b) linear correlation coefficient between the 200-mb MJO advective tendency anomaly and zonal wind anomaly averaged between 150° and 160°E for 15 years (1979–93) of NCEP (solid line) and ECMWF (dashed line) reanalyses data.

damping comes equally from the advective tendency (the nonlinear meridional advection term) and X. The linear correlation coefficients (Figs. 11b,d,f) are generally large when the regression coefficient are large, suggesting the usefulness of linear damping representation.

Since the damping involves mean flow, its value varies in space. For example, Fig. 12 shows the meridional distribution at 200 mb of damping due to the advective tendency, in longitudes 150°–160°. The damping is large only near the equator between 10°N and 10°S because the strong upper-level zonal divergence and vertical motion are confined near the equator. The damping in the lower levels also has its largest value near the equator (not shown).

As mentioned in section 3, deep convection signal in the MJO has two centers of variance: western Pacific and eastern Indian Ocean. The above results are for the western Pacific. We also did similar analysis for the eastern Indian Ocean. The wave structures and zonal momentum budgets in the eastern Indian Ocean are generally similar to those in the western Pacific except during the boreal summer (not shown). Many previous studies have shown that the boreal summer intraseasonal oscillation has a prominent northward-propagating component (e.g., Yasunari 1979; Madden and Julian 1994), which is different from the eastward-propagating MJO mode originally described by Madden and Julian (1971, 1972), although there are some connections between the northward-propagating mode and the eastward-propagating MJO mode (Lawrence and Webster 2002). Therefore we restrict this study to the eastward-propagating MJO mode and will report the results for the boreal summer intraseasonal oscillation in a separate study.

5. Summary and discussions

The observed MJO wave structure and zonal momentum budget at the equator are schematically shown in Fig. 13. The equatorial wave structure of the MJO is associated with a vertical mode concentrated in the upper half of the troposphere, with middle-troposphere inflow and near-tropopause outflow at the time of maximum precipitation. The vertical motion has a westward phase tilt with height, but zonal divergence is offset to the east of the ascent by meridional effects (Rossby wave flow components), making it slightly difficult to display both tilts with a schematic circulation in the zonal plane. The main feature to note here is that geopotential height lags zonal wind by about 5–10 days at both the inflow and outflow layers.

In the MJO zonal momentum budget, the advective tendency is a major budget term in both upper and lower troposphere, while subgrid transports are a major budget term only in the lower troposphere. The advective tendency in the upper troposphere comes from linear terms associated with time-mean zonal and vertical motions, while that in the lower troposphere comes from zonal mean linear meridional advection. The simplified MJO zonal momentum equation is Eq. (8).

The strong linear advection terms in the upper troposphere can be understood from the time-mean flow in the warm-pool region where abundant climatological deep convection is associated with strong upward motion ($[\omega] < 0$), upper-level zonal divergence ($\partial[u]/\partial x > 0$), and mean upper-level easterly wind ($[u] < 0$). When the MJO travels in such a large-scale environment, at the upper levels, $-[u]\partial u'/\partial x$ lags u' by a quarter cycle, while both $-u'\partial[u]/\partial x$ and $-[\omega]\partial u'/\partial p$ are out of phase with u'. Given the low frequency of the MJO, the magnitudes of the time-mean flows are bound to cause an advective tendency much larger than the local tendency. The advective tendency and convective eddy momentum flux convergence together provide a 3–5-day time-scale damping to the MJO both in the upper troposphere and in the lower troposphere. Therefore,

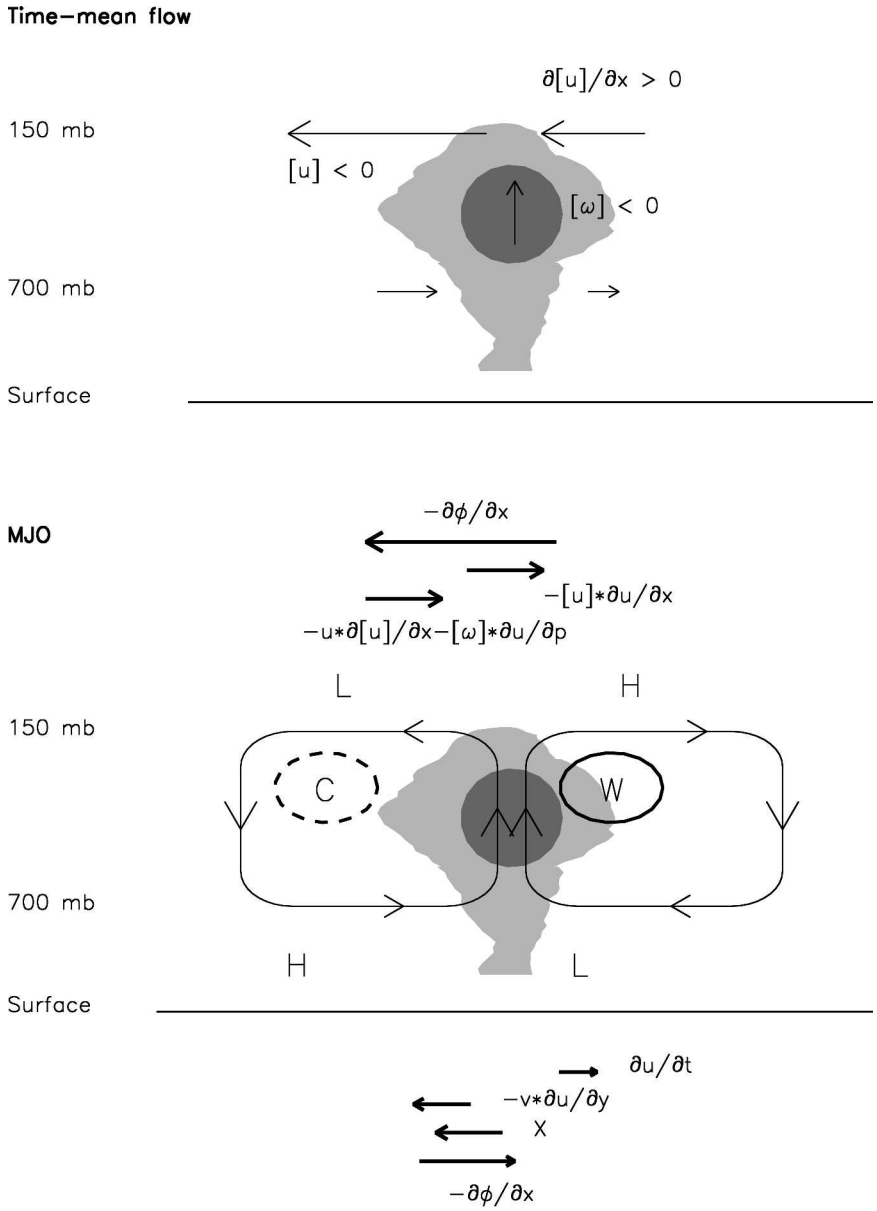

FIG. 13. Schematic depiction of the time-mean flow over the warm-pool and the observed MJO wave structure and zonal momentum budget. Regions of enhanced large-scale convection are indicated schematically by the clouds. The dark shading inside the clouds represents the maximum of the diabatic heating. "H" and "L" represent the high and low geopotential height anomalies, respectively. "W" inside thick solid circle and "C" inside thick dashed circle represent the warm and cold temperature anomalies, respectively. Thin arrows represent the winds. Thick arrows above the MJO wave represent components of zonal momentum budget in the upper troposphere, while those below the MJO wave represent components in the lower troposphere.

the MJO is a highly viscous oscillation. At western Pacific longitudes, the damping is large only near the equator between 10°N and 10°S. The full 3D spatial structure of mean flow may constitute a spatial envelope that shapes the MJO importantly, but the assumptions behind linearized composite diagnostics here do not warrant production of detailed maps of damping rates.

It may be possible to anticipate the effect of the observed strong damping on theoretical models of intraseasonal oscillations. The possible effects are threefold.

First, strong mechanical damping may directly affect

growth rates and phase speed. One obvious effect is to reduce growth rates, perhaps stabilizing unstable modes found under weak-damping assumptions, for example as shown in the WISHE model of Goswami and Rao (1994, their Fig. 5c). It may require several positive feedback mechanisms to generate unstable modes in the presence of damping (e.g., WISHE plus cloud–radiation feedback). Another possible effect is on the phase speed of intraseasonal modes. For example, the wave–CISK model of Chao (1987) shows that strong damping reduces phase speed. Phase speed or period will also be importantly affected by quadrature terms like $-[\bar{u}]\partial\tilde{u}'/\partial x$, which might be more conveniently viewed as a simple Doppler shifting by the mean flow.

Second, strong mechanical damping may also affect the thermodynamic structure and thus the wave-convection feedback. We have seen that the existence of warm-pool mean flow necessitates baroclinic Z' anomalies in the MJO, in order to sustain the zonally divergent zonal wind anomalies associated with its low-frequency convection anomalies. These Z' anomalies correspond to temperature anomalies, as indicated on Fig. 13. Specifically, the lowness of MJO frequency relative to the time scale of mean-flow advective damping forces the warm anomaly ahead of the convection to shift rearward, into the convective heating anomaly.

In the terms of a conventional short-hand of energetics reasoning (e.g., Emanuel et al. 1994), this phase shift tends to increase the correlation between heating and temperature, thus increasing eddy energy production. It is tempting to claim that this reasoning might comprise an explanation for the enhanced power in low frequencies that we call the MJO, or an interpretation of the constant-frequency rather than dispersion-line spectral characteristics of the MJO (Wheeler and Kiladis 1999). But circumspection requires acknowledging that the spatial correlation in the equatorial zonal plane between time-filtered zonal deviations of heating and temperature is at best a very partial study of the energetics of observed variability, and falls far short of a useful predictive theory of why that observed variability exists.

Nonetheless, this study points to the fact that the presence of mean wavy basic state (the strong mean flow over the Indo–Pacific warm pool) significantly affects both the dynamical and the thermodynamical structures of the MJO. Such effects were missing in the aquaplanet type experiments conducted by some previous GCM studies of the MJO (e.g., Hayashi and Sumi 1986; Swinbank et al. 1988; Lau et al. 1988; Tokioka et al. 1988; Lee et al. 2001). When zonally symmetric basic state was assumed, the very weak mean flow lead to very weak advective tendency, so the zonal momentum balance for the simulated intraseasonal mode is between local tendency and pressure gradient force, resulting in an in-phase relationship between zonal wind and geopotential height anomalies (see discussions in Lau et al. 1988). Therefore the upper-level geopotential height anomaly (and the temperature anomaly) tend to lead the low-level convergence anomaly (and the heating anomaly) by a quarter cycle, a configuration inefficient for eddy energy production. Actually, a westward tilt with height of the wave structure is needed to make the temperature positively correlated with heating. Our results, however, demonstrate that with the presence of mean wavy basic state (the strong mean flow over the Indo–Pacific warm pool), the advective tendency can help to shift the temperature anomaly backward into the heating anomaly, leading to a more efficient eddy energy production. This provides an alternate eddy energy production mechanism in addition to westward phase tilt in wave structure. It is in line with the findings of Slingo et al. (1996) from the Atmospheric Model Intercomparison Project (AMIP) that GCMs that produce more realistic intraseasonal variability also tend to produce stronger and deeper time-mean vertical motion. It is clear that the effort to improve intraseasonal variability in global models must be considered in concert with the effort to simulate the mean climate well.

Finally, as discussed in the introduction, the equivalent linear damping between the surface and 850 mb is important for the frictional Wave–CISK mechanism (e.g., Wang and Rui 1990a; Wang and Li 1994; Moskowitz and Bretherton 2000). Figure 11e shows that eddy flux convergence alone provides a 3-day damping at 925 mb and a 6-day damping at 850 mb. Since the subcloud turbulent layer typically does not extend above 940 mb, this suggests a possibly important role for CMT by shallow convection, which is consistent with the finding of Carr and Bretherton (2001) from seasonal mean momentum budget. The frictional layer is therefore significantly thicker than the subcloud turbulent layer. As shown by Wang and Li (1994), the growth rate of the frictional wave–CISK mode increases quickly with the thickness of the frictional layer. Interestingly, CMT by shallow convection has not been included in many GCMs, and including it may help to destablize the MJO-like modes.

We can compare our estimated equivalent linear damping rate in the frictional layer with those used in frictional Wave–CISK models. Figures 11e and 11c show that eddy flux convergence and advective tendency together provide a equivalent damping rate of about 1.2 day at 1000 mb, gradually reducing to about 3.5 day at 850 mb (Figs. 11c,e). Note in the models, a well-mixed frictional layer is generally assumed. Wang and Rui (1990a) used a 0.3-day linear damping for a 100-mb-thick frictional layer, and a 0.51-day damping for a 150-mb-thick frictional layer. The damping rates are stronger than our estimates from observation. Moskowitz and Bretherton (2000) used a 1.3-day linear damping for a 50-mb-thick frictional layer. The damping rate is similar to our estimates, but their frictional layer seems too thin. So our observational estimates fall

in between those two models, and we cannot rule out the potential importance of frictional wave–CISK to the amplification of the MJO.

It is important to note that the equivalent linear damping estimated in the present study is the damping in the momentum equation, not that in the kinetic energy equation. In terms of the kinetic energy budget, the modeling study by Yano and Emanuel (1991) demonstrated that wave radiation into the stratosphere is an important mechanism for damping the wave. Because the upward group velocity is larger for smaller zonal wavelengths, short waves in the troposphere are strongly damped and the most unstable mode shifts to low wavenumbers. This constitutes a promising mode-selection mechanism and we are planning to test it using observational data in the future.

Acknowledgments. The authors are very grateful to Klaus Weickmann and George Kiladis for carefully reading an early version of the manuscript and making very helpful comments; to Dave Randall, Chris Bretherton, Bin Wang, Andy Majda, Adam Sobel, Winston Chao, and Toshio Yamagata for helpful discussions; and to Kerry Emanuel and two anonymous reviewers for valuable reviews. We also thank Don Hooper for assistance in reading the reanalyses data. This work was supported by the National Science Foundation Grants ATM-0097116, ATM-0073206, and ATM-0112715, and by NOAA OGP and U.S. CLIVAR CMEP.

APPENDIX

Decomposition of the Advection Terms

Because the MJO anomaly in this study does not include the zonal mean, decomposition of the advection terms is more complex than when zonal mean is retained. Following Peixoto and Oort (1992, 61–64), a quantity A can be decomposed into

$$A = [\overline{A}] + [\tilde{A}] + \overline{A}' + \tilde{A}', \tag{A1}$$

where overbar represents zonal mean, tilde represents deviation from the zonal mean (zonal asymmetric component), bracket represents time mean, and prime represents deviation from the time mean. It can be derived that

$$\begin{aligned}\widetilde{AB}' = {} & ([\tilde{A}]\tilde{B}' + [\tilde{B}]\tilde{A}') + ([\overline{A}]\tilde{B}' + [\overline{B}]\tilde{A}') \\ & + ([\tilde{A}]\overline{B}' + [\tilde{B}]\overline{A}') \\ & + (-\overline{[\tilde{A}]\tilde{B}'} - \overline{[\tilde{B}]\tilde{A}'} + \widetilde{A'B'} - [\widetilde{A'B'}]).\end{aligned} \tag{A2}$$

On the right-hand side of the equation, the terms on the first line are the linear terms, among which the first two are associated with time-mean zonal asymmetric component, and are calculated in Eqs. (5) and (7). The third and fourth are associated with time-mean zonal-mean component. The fifth and sixth are associated with temporally filtered zonal-mean component. The terms on the second line are the nonlinear terms. When considering only the 30–70-day anomalies, the nonlinear terms will include some more terms corresponding to interaction with other time scales.

REFERENCES

Bantzer, C. H., and J. M. Wallace, 1996: Intraseasonal variability in tropical mean temperature and precipitation and their relation to the tropical 40–50-day oscillation. *J. Atmos. Sci.,* **53,** 3032–3045.

Bergman, J. W., H. H. Hendon, and K. M. Weickmann, 2001: Intraseasonal air–sea interactions at the onset of El Niño. *J. Climate,* **14,** 1702–1719.

Blade, I., and D. L. Hartmann, 1993: Tropical intraseasonal oscillations in a simple nonlinear model. *J. Atmos. Sci.,* **50,** 2922–2939.

Carr, M. T., and C. S. Bretherton, 2001: Convective momentum transport over the tropical Pacific: Budget estimates. *J. Atmos. Sci.,* **58,** 1673–1693.

Chang, C. P., 1977: Viscous internal gravity waves and low-frequency oscillations in the tropics. *J. Atmos. Sci.,* **34,** 901–910.

——, and H. Lim, 1988: Kelvin wave-CISK: A possible mechanism for the 30–50 day oscillations. *J. Atmos. Sci.,* **45,** 1709–1720.

Chao, W. C., 1987: On the origin of the tropical intraseasonal oscillation. *J. Atmos. Sci.,* **44,** 1940–1949.

Duchan, C. E., 1979: Lanczos filtering in one and two dimensions. *J. Appl. Meteor.,* **18,** 1016–1022.

Emanuel, K. A., 1987: An air–sea interaction model of intraseasonal oscillation in the Tropics. *J. Atmos. Sci.,* **44,** 2324–2340.

——, J. D. Neelin, and C. S. Bretherton, 1994: On large-scale circulations in convecting atmospheres. *Quart. J. Roy. Meteor. Soc.,* **120,** 1111–1143.

Esbensen, S. K., E. I. Tollerud, and J.-H. Chu, 1982: Cloud-cluster-scale circulations and the vorticity budget of synoptic-scale waves over the eastern Atlantic intertropical convergence zone. *Mon. Wea. Rev.,* **110,** 1677–1692.

Gibson, J. K., P. Kållberg, S. Uppala, A. Hernandez, A. Nomura, and E. Serrano, 1997: ERA description. ECMWF Reanalysis Project Report Series 1, 86 pp.

Gill, A. E., 1980: Some simple solutions for heat-induced tropical circulation. *Quart. J. Roy. Meteor. Soc.,* **106,** 447–462.

Goswami, P., and R. K. Rao, 1994: A dynamical mechanism for selective excitation of the Kelvin mode at timescale of 30–50 days. *J. Atmos. Sci.,* **51,** 2769–2779.

Haertel, P. T., and G. N. Kiladis, 2004: Dynamics of 2-day equatorial waves. *J. Atmos. Sci.,* **61,** 2707–2721.

Hayashi, Y., and D. G. Golder, 1986: Tropical intraseasonal oscillations appearing in a GFDL general circulation model and FGGE data. Part I: Phase propagation. *J. Atmos. Sci.,* **43,** 3058–3067.

——, and A. Sumi, 1986: The 30–40 day oscillation simulated in an "aqua planet" model. *J. Meteor. Soc. Japan,* **64,** 451–466.

——, and D. G. Golder, 1988: Tropical intraseasonal oscillations appearing in a GFDL general circulation model and FGGE data. Part II: Structure. *J. Atmos. Sci.,* **45,** 3017–3033.

——, and ——, 1993: Tropical 40–50- and 25–30-day oscillations appearing in realistic and idealized GFDL climate models and the ECMWF dataset. *J. Atmos. Sci.,* **50,** 464–494.

——, and ——, 1997: United mechanisms for the generation of low- and high-frequency tropical waves. Part I: Control ex-

periments with moist convective adjustment. *J. Atmos. Sci.,* **54,** 1262–1276.

Hendon, H. H., and B. Liebmann, 1990: A composite study of onset of the Australian summer monsoon. *J. Atmos. Sci.,* **47,** 2227–2240.

Higgins, R. W., and K. C. Mo, 1997: Persistent North Pacific circulation anomalies and the tropical intraseasonal oscillation. *J. Climate,* **10,** 223–244.

——, J.-K. E. Schemm, W. Shi, and A. Leetmaa, 2000: Extreme precipitation events in the western United Stated related to tropical forcing. *J. Climate,* **13,** 793–820.

Houze, R. A., Jr., S. S. Chen, D. E. Kingsmill, Y. Serra, and S. E. Yuter, 2000: Convection over the Pacific warm pool in relation to the atmospheric Kelvin–Rossby wave. *J. Atmos. Sci.,* **57,** 3058–3089.

Hsu, H.-H., 1996: Global view of the intraseasonal oscillation during northern winter. *J. Climate,* **9,** 2386–2406.

Kalnay, E., and Coauthors, 1996: The NCEP/NCAR 40-Year Reanalysis Project. *Bull. Amer. Meteor. Soc.,* **77,** 437–471.

Kessler, W. S., M. J. McPhaden, and K. M. Weickmann, 1995: Forcing of intraseasonal Kelvin waves in the equatorial Pacific. *J. Geophys. Res.,* **100,** 10 613–10 631.

Kiladis, G. N., and K. M. Weickmann, 1992: Circulation anomalies associated with tropical convection during northern winter. *Mon. Wea. Rev.,* **120,** 1900–1923.

——, K. H. Straub, and P. T. Haertel, 2005: Zonal and vertical structure of the Madden–Julian oscillation. *J. Atmos. Sci.,* in press.

Knutson, T. R., and K. M. Weickmann, 1987: 30–60 day atmospheric oscillations: Composite life cycles of convection and circulation anomalies. *Mon. Wea. Rev.,* **115,** 1407–1436.

Lau, K. M., and P. H. Chan, 1985: Aspects of the 40–50-day oscillation during the northern winter as inferred from outgoing longwave radiation. *Mon. Wea. Rev.,* **113,** 1889–1909.

——, and T. J. Phillips, 1986: Coherent fluctuations of extratropical geopotential height and tropical convection in intraseasonal timescales. *J. Atmos. Sci.,* **43,** 1164–1181.

——, and L. Peng, 1987: Origin of low-frequency (intraseasonal) oscillations in the tropical atmosphere. *J. Atmos. Sci.,* **44,** 950–972.

Lau, N. C., I. M. Held, and J. D. Neelin, 1988: The Madden–Julian oscillations in an idealized general circulation model. *J. Atmos. Sci.,* **45,** 3810–3831.

Lawrence, D. M., and P. J. Webster, 2002: The boreal summer intraseasonal oscillation: Relationship between northward and eastward movement of convection. *J. Atmos. Sci.,* **59,** 1593–1606.

Lee, M.-I., I.-S. Kang, J.-K. Kim, and B. E. Mapes, 2001: Influence of cloud–radiation interaction on simulating tropical intraseasonal oscillation with an atmospheric general circulation model. *J. Geophys. Res.*, **106,** 14 219–14 233.

Liebmann, B., H. H. Hendon, and J. D. Glick, 1994: The relationship between tropical cyclones of the western Pacific and Indian Oceans and the Madden–Julian oscillation. *J. Meteor. Soc. Japan,* **72,** 401–411.

Lin, J. L., and B. E. Mapes, 2004: Radiation budget of the tropical intraseasonal oscillations. *J. Atmos. Sci.,* **61,** 2050–2062.

——, ——, M. H. Zhang, and M. Newman, 2004: Stratiform precipitation, vertical heating profiles, and the Madden–Julian oscillation. *J. Atmos. Sci.,* **61,** 296–309.

Madden, R. A., and P. R. Julian, 1971: Detection of a 40–50 day oscillation in the zonal wind in the tropical Pacific. *J. Atmos. Sci.,* **28,** 702–708.

——, and ——, 1972: Description of global-scale circulation cells in the tropics with a 40–50 day period. *J. Atmos. Sci.,* **29,** 1109–1123.

——, and ——, 1994: Observations of the 40–50-day oscillation—A review. *Mon. Wea. Rev.,* **122,** 814–837.

Moskowitz, B. M., and C. S. Bretherton, 2000: An analysis of frictional feedback on a moist equatorial Kelvin mode. *J. Atmos. Sci.,* **57,** 2188–2206.

Murakami, M., 1979: Large-scale aspects of deep convective activity over the GATE area. *Mon. Wea. Rev.,* **107,** 994–1013.

Nakazawa, T., 1986: Mean features of 30–60 day variations as inferred from 8-year OLR data. *J. Meteor. Soc. Japan,* **64,** 777–786.

Neelin, J. D., and J.-Y. Yu, 1994: Modes of tropical variability under convective adjustment and the Madden–Julian oscillation. Part I: Analytical theory. *J. Atmos. Sci.,* **51,** 1876–1894.

——, I. M. Held, and K. H. Cook, 1987: Evaporation–wind feedback and low-frequency variability in the tropical atmosphere. *J. Atmos. Sci.,* **44,** 2341–2348.

Oort, A. H., and J. J. Yienger, 1996: Observed long-term variability in the Hadley circulation and its connection to ENSO. *J. Climate,* **9,** 2751–2767.

Peixoto, J. P., and A. H. Oort, 1992: *Physics of Climate*. American Institute of Physics, 520 pp.

Raymond, D. J., 2001: A new model of the Madden–Julian oscillation. *J. Atmos. Sci.,* **58,** 2807–2819.

Reed, R. J., and R. H. Johnson, 1974: The vorticity budget of synoptic-scale wave disturbances in the tropical western Pacific. *J. Atmos. Sci.,* **31,** 1784–1790.

Salby, M. L., and H. H. Hendon, 1994: Intraseasonal behavior of clouds, temperature, and motion in the Tropics. *J. Atmos. Sci.,* **51,** 2207–2224.

——, R. B. Garcia, and H. H. Hendon, 1994: Planetary-scale circulations in the presence of climatological and wave-induced heating. *J. Atmos. Sci.,* **51,** 2344–2367.

Shapiro, L. J., 1978: The vorticity budget of a composite African tropical wave disturbance. *Mon. Wea. Rev.,* **106,** 806–817.

Slingo, J. M., and Coauthors, 1996: Intraseasonal oscillations in 15 atmospheric general circulation models: Results from an AMIP diagnostic subproject. *Climate Dyn.,* **12,** 325–357.

Stevens, D. E., 1979: Vorticity, momentum, and divergence budgets of synoptic-scale wave disturbances in the tropical eastern Atlantic. *Mon. Wea. Rev.,* **107,** 535–550.

Sui, C.-H., and M. Yanai, 1986: Cumulus ensemble effects on the large-scale vorticity and momentum fields of GATE. Part I: Observational evidence. *J. Atmos. Sci.,* **43,** 1618–1642.

Swinbank, R. T., N. Palmer, and M. K. Davey, 1988: Numerical simulations of the Madden and Julian oscillation. *J. Atmos. Sci.,* **45,** 774–788.

Takayabu, Y. N., T. Iguchi, M. Kachi, A. Shibata, and H. Kanzawa, 1999: Abrupt termination of the 1997–98 El Niño in response to a Madden–Julian oscillation. *Nature,* **402,** 279–282.

Tokioka, T., K. Yamazaki, A. Kitoh, and T. Ose, 1988: The equatorial 30–60-day oscillation and the Arakawa–Schubert penetrative cumulus parameterization. *J. Meteor. Soc. Japan,* **66,** 883–901.

Tung, W. W., and M. Yanai, 2002a: Convective momentum transport observed during the TOGA COARE IOP. Part I: General features. *J. Atmos. Sci.,* **59,** 1857–1871.

——, and ——, 2002b: Convective momentum transport observed during the TOGA COARE IOP. Part II: Case studies. *J. Atmos. Sci.,* **59,** 2535–2549.

Wang, B., 1988: Dynamics of tropical low-frequency waves: An analysis of the moist Kelvin wave. *J. Atmos. Sci.,* **45,** 2051–2065.

——, and H. Rui, 1990a: Dynamics of the coupled moist Kelvin–Rossby wave on an equatorial β-plane. *J. Atmos. Sci.,* **47,** 397–413.

——, and ——, 1990b: Synoptic climatology of transient tropical intraseasonal convection anomalies. *Meteor. Atmos. Phys.,* **44,** 43–61.

——, and T. Li, 1994: Convective interaction with boundary-layer

dynamics in the development of a tropical intraseasonal system. *J. Atmos. Sci.,* **51,** 1386–1400.

Weickmann, K. M., G. R. Lussky, and J. E. Kutzbach, 1985: Intraseasonal (30–60 day) fluctuations of outgoing longwave radiation and 250 mb streamfunction during northern winter. *Mon. Wea. Rev.,* **113,** 941–961.

——, G. N. Kiladis, and P. D. Sardeshmukh, 1997: The dynamics of intraseasonal atmospheric angular momentum oscillations. *J. Atmos. Sci.,* **54,** 1445–1461.

Wheeler, M., and G. N. Kiladis, 1999: Convectively coupled equatorial waves: Analysis of clouds and temperature in the wavenumber–frequency domain. *J. Atmos. Sci.,* **56,** 374–399.

Xie, P., and P. A. Arkin, 1997: Global precipitation: A 17-year monthly analysis based on gauge observations, satellite estimates, and numerical model outputs. *Bull. Amer. Meteor. Soc.,* **78,** 2539–2558.

Xie, S.-P., 1994: On the preferred zonal scale of wave-CISK with conditional heating. *J. Meteor. Soc. Japan,* **72,** 19–30.

Yano, J. I., and K. A. Emanuel, 1991: An improved model of the equatorial troposphere and its coupling with the stratosphere. *J. Atmos. Sci.,* **48,** 377–389.

Yasunari, T., 1979: Cloudiness fluctuations associated with the northern hemisphere summer monsoon. *J. Meteor. Soc. Japan,* **57,** 227–242.